Revue des Composites et des Matériaux Avancés-Journal of Composite and Advanced Materials
Vol. 36, No. 5, October, 2026, pp. 1093-1101
Journal homepage: http://iieta.org/journals/rcma

Combined Effects of Particle Size and Walnut Shell Powder Content on the Tensile and Compressive Mechanical Properties of Epoxy Composites: Experimental Study and Micromechanical Modeling

S. Loukmane[1*], A. Lamarti[2,3], A. Hachim[2,3], B. Kissi[1]

[1] Laboratory of Complex Cyber Physical Systems, the Higher National School of Arts and Crafts-Casablanca (ENSAM), Hassan II University, Casablanca 20670, Morocco
[2] Laboratory of Mechanics, Engineering, and Innovation, National Higher School of Electricity and Mechanics (ENSEM), Hassan II University, Casablanca 20200, Morocco
[3] Higher Institute for Maritime Studies (ISEM), Casablanca 20200, Morocco

Corresponding Author Email: loukmanesalaheddine@gmail.com

Copyright: ©2026 The authors. This article is published by IIETA and is licensed under the CC BY 4.0 license (http://creativecommons.org/licenses/by/4.0/).

https://doi.org/10.18280/rcma.360515

Received: 6 July 2026
Revised: 30 August 2026
Accepted: 20 September 2026
Available online: 31 October 2026

Keywords:
bio-based composite, epoxy resin, Halpin–Tsai, mechanical properties, micromechanical models, particle size, Pukánszky, walnut shell powder

ABSTRACT

This study evaluates the combined effect of particle size (100, 200, 400 µm) and filler content (10, 25, 40 wt.%) of untreated walnut shell powder on the tensile and compressive performance of epoxy composites, and tests the validity of Halpin–Tsai and Pukánszky models. Tensile and compressive tests followed ASTM D638 and D695. Experimental results show that increasing filler content raises Young's modulus (up to + 77% at 40 wt.% with 100 µm particles) but reduces tensile strength. Under compression, analysis of variance (ANOVA) revealed that particle size and filler content are highly significant ($p < 0.001$): 100 µm particles maintain relative ductility (57.9–62.9 MPa), while 400 µm particles cause brittle failure beyond 25 wt.%. Pukánszky model correlates better with experimental data (deviation +0.3% to −11.8%) than Halpin–Tsai (up to −55%). The best compromise is obtained with 100 µm particles, which improve stiffness while preserving ductile compressive behaviour, highlighting interfacial adhesion as the key factor for optimizing bio-based composites.

1. INTRODUCTION

Bio-based composites are increasingly studied for sustainability and circular economy, especially through valorisation of agri-food by-products in polymer matrices [1-3]. Epoxy resins, known for their mechanical properties and chemical stability, are often blended with lignocellulosic fillers to reduce environmental footprint while tailoring performance [4, 5].

Walnut shell powder (*Juglans regia* L.) is abundant, low density, and lignocellulosic [6-8]. Recent studies show it can reinforce epoxy matrices when particle size and mass fraction are controlled [9-14]. Three sizes were selected: 100, 200, and 400 µm. This range covers practical sieve thresholds and matches literature on walnut shell/epoxy composites [9, 11, 12]. Chaoufi et al. [15] found an optimum at 10 wt.% for date palm nut powder/epoxy composites, highlighting the role of filler origin and morphology.

The literature shows inconsistencies. Finer particles generally improve stiffness and load transfer [11], but high filler fractions cause agglomeration and interfacial debonding, reducing strength [9, 12]. Few studies systematically explore combined particle size and content under both tensile and compressive loading. Experimental validation of Halpin–Tsai and Pukánszky models remains scarce for these systems.

This study investigates three particle sizes (100, 200, 400 µm) and three weight fractions (10, 25, 40 wt.%) on the tensile and compressive performance of walnut shell/epoxy composites. It also assesses the predictive capability of Halpin–Tsai and Pukánszky models to identify favourable formulation parameters.

2. MATERIALS AND METHODS

2.1 Materials

2.1.1 The epoxy matrix

The matrix is a two-component ECO epoxy resin (EPODEX), mixed at a 2:1 ratio. Properties: density 1.10 g·cm^{-3}, viscosity 700 MPa·s, Shore D hardness 87 [16].

2.1.2 Reinforcement: Walnut shell powder

Walnut shells (*Juglans regia* L.) were cleaned, dried at 70 ± 1 °C for 3 h, ground in a stainless steel rotary mill, and sieved through square-mesh sieves using a mechanical shaker (10 min, 300 shakes/min) to obtain three fractions: 100, 200, and 400 µm. True density is 0.692 g·cm^{-3} [7]. Residual moisture, determined by loss on drying at 105 ± 2 °C for 3 h (European Pharmacopoeia 2.2.32), was about 2 wt.% [17]. Particles are

irregular, angular, and rough, typical of ground lignocellulosic fillers. Figure 1 illustrates the complete preparation process, including cleaning and drying, crushing, powder drying to reduce moisture, and sieving. Chemical composition is based on literature data [18, 19]. Table 1 summarizes typical walnut shell composition. A more detailed characterization (quantitative particle size distribution, specific surface area, scanning electron microscopy (SEM)) was not performed due to equipment limitations and will be addressed in future work.

Table 1. Chemical composition of walnut shell (*Juglans regia* L.) based on literature data

Type of Shell	Cellulose (wt.%)	Hemicellulose (wt.%)	Lignin (wt.%)	Ash/Extractives (wt.%)
Walnut shell	23.9	22.4	50.3	3.4

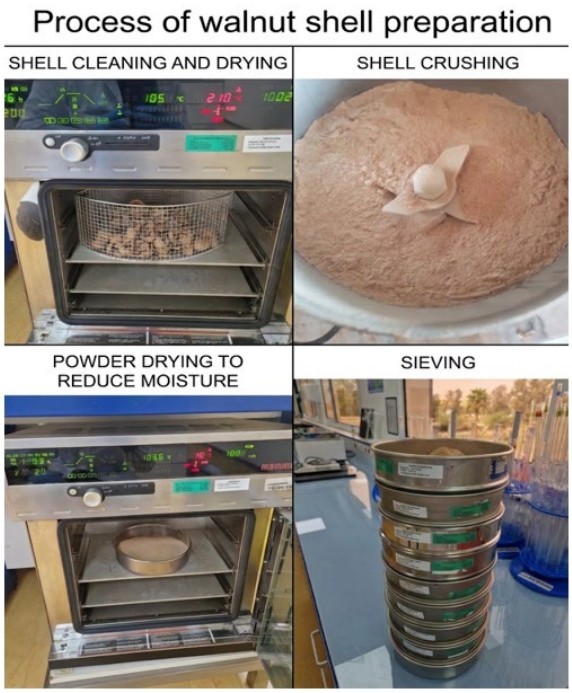


Figure 1. Walnut shell preparation process: (a) cleaning and drying, (b) crushing, (c) powder drying to reduce moisture, and (d) sieving

2.2 Composite processing

Composites were prepared with 10, 25, and 40 wt.% filler for each particle size, plus neat epoxy (0%). Powder was manually mixed into resin with a spatula for 10 min; hardener was added (2:1) and mixed for 5 min. The mixture was cast into silicone molds (ASTM D638 and D695) [20, 21]. After casting, bubbles were allowed to rise, and a hot air torch (15–20 cm) was passed over the surface to remove them. No vacuum degassing was used. Dispersion was visually inspected; no macroscopic agglomerates were observed. Curing: 23 ± 2 °C for 72 h, then 7-day conditioning. Figure 2 shows the fabrication steps.

2.3 Conversion of mass fractions to volume fractions

Volume fractions were calculated using Eq. (1).

$$V_f = \frac{\omega_f/\rho_f}{\left[\left(\frac{\omega_f}{\rho_f}\right)+\left(\frac{\omega_m}{\rho_m}\right)\right]} \quad (1)$$

where, V_f is the volume fraction of the reinforcement, ω_f is the mass fraction of the reinforcement, ω_m is the mass fraction of the matrix, ρ_f is the density of the reinforcement, and ρ_m is the density of the matrix. The volume fraction of the matrix is given by Eq. (2).

$$V_m = 1 - V_f \quad (2)$$

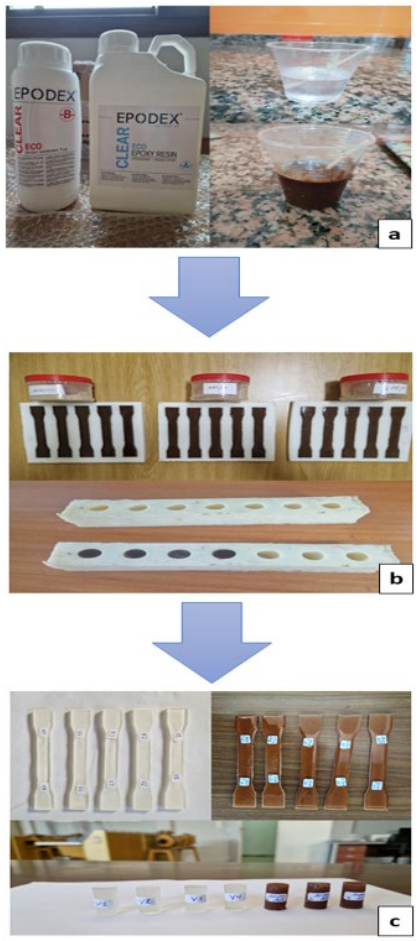


Figure 2. Composite fabrication process: (a) manual mixing of resin and walnut shell powder, (b) casting into silicone molds, and (c) demolded final specimens after curing

Table 2. Coding of the formulations and corresponding volume fractions

Code	Mass Fraction (%)	Particle Size (µm)	V_f
E0	0	—	0
E10-100	10	100	0.150
E10-200	10	200	0.150
E10-400	10	400	0.150
E25-100	25	100	0.346
E25-200	25	200	0.346
E25-400	25	400	0.346
E40-100	40	100	0.515
E40-200	40	200	0.515
E40-400	40	400	0.515

The coding of the formulations was defined according to the filler weight percentage and the powder particle size, as presented in Table 2.

2.4 Mechanical testing

2.4.1 Tensile tests

Tensile tests are performed according to ASTM D638 [20] on type I specimens, at a crosshead speed of 5 mm·min⁻¹ on a 30 kN capacity machine, under controlled conditions. Five specimens per formulation (n = 5) are tested until failure. The tensile strength at break, Young's modulus (determined by linear regression between 0.05% and 0.25% strain), and elongation at break are calculated from the stress strain curves. Results are reported as mean ± standard deviation.

2.4.2 Compression tests

Compression tests are performed according to ASTM D695 [21] on an RP 25 ATF machine (25 kN capacity), at a crosshead speed of 1 mm·min⁻¹, on cylindrical specimens (25.4 mm length × 12.7 mm diameter) cast in silicone molds at 23 ± 2 °C. Figure 3 shows a typical specimen mounted between the grips of the universal testing machine during compression testing. Five specimens per formulation (n = 5) are tested until failure.



Figure 3. Compression test on a cylindrical specimen according to the ASTM D695 standard [21] using a universal testing machine

2.5 Statistical analysis

Two-way analysis of variance (ANOVA) was applied to maximum compressive stress due to non-monotonic trends for 400 µm particles and ductile–brittle transition. Factors: filler content (10, 25, 40%) and particle size (100, 200, 400 µm), with n = 5 (45 observations). Normality (Shapiro–Wilk) and variance homogeneity (Bartlett) were checked at α = 0.05. ANOVA with interaction was followed by Tukey's honestly significant difference (HSD) post-hoc test. Letter groupings (a, b, c) indicate no significant difference at 5%. For tensile tests, a descriptive analysis was preferred because the study focuses on micromechanical modeling rather than statistical inference. Tensile trends are monotonic with low standard deviations relative to differences between formulations. Moreover, the compression ANOVA confirmed the significance of both factors and their interaction, and the same factors govern tensile behaviour. A full statistical evaluation of tensile data will be included in future work.

2.6 Theoretical modeling

2.6.1 Prediction of the elastic modulus: Halpin–Tsai model

The elastic modulus of the composite is modeled using the Halpin–Tsai model [22]. This model was selected for its simplicity and its low data requirements, which are advantageous in the absence of detailed microstructural characterization. The reinforcement geometry is incorporated through a shape parameter ξ, with spherical particles assumed (ξ = 2), a value validated by recent studies [23]. Young's modulus is given by Eq. (3).

$$E_c = E_m\left(\frac{1 + \xi\eta V_f}{1 - \eta V_f}\right) \tag{3}$$

with:

$$\eta = \frac{\frac{E_f}{E_m} - 1}{\frac{E_f}{E_m} - \xi} \tag{4}$$

The epoxy matrix has a Young's modulus E_m = 524.6 MPa and a density ρ_m = 1.10 g·cm⁻³. The walnut shell particles are spherical, with a modulus E_f = 5.2 GPa [19] and a true density ρ_f = 0.692 g·cm⁻³ [18]. The mass fractions studied are 10, 25, and 40%. The assumptions of the study include spherical particles, homogeneous dispersion, perfect interfacial adhesion, and an isotropic composite.

It should be noted, however, that the actual particles are angular and irregular, and the interface is untreated, meaning these assumptions are not fully met. These simplifications tend to overestimate the modulus, especially at high filler contents, as discussed in Section 4.3.

2.6.2 Prediction of the tensile strength: Pukánszky model

Tensile strength is modeled using Pukánszky's semi-empirical model [24]. This model was chosen because it is designed to analyze the ultimate tensile properties of filled polymer composites and is formulated for quasi-spherical particle fillers, which aligns with the assumptions of this study. Eq. (5) represents the stress, where σ_m is the tensile strength of the pure epoxy matrix, and σ_c is that of the composite.

$$\sigma_c = \sigma_m\left(\frac{1 - V_f}{1 + 2.5V_f}\exp(BV_f)\right) \tag{5}$$

The parameter B is not a conventional constant; it is influenced by several factors such as the interface, charge transfer, particle aggregation, and the microstructure of the composite [25]. Recent studies have correlated it with interfacial shear strength (IFSS) [25, 26]. For methodological reasons, a parameter B specific to each particle size (100, 200, and 400 µm) was determined by linear regression (ordinary least squares method) based on the experimental results of tensile tests. The values obtained are presented in Table 3.

Table 3. The interaction parameter B in the Pukánszky model, expressed in terms of particle size

Particle Size (µm)	B
100	1.689
200	1.222
400	0.827

The values of B were substituted into Eq. (5) to calculate the theoretical resistances of the composites for each particle size.

3. RESULTS

3.1 Tensile mechanical properties

Table 4 presents the tensile properties of the tested composites. Pure epoxy (E0) exhibited an average tensile strength of 34.56 ± 4.47 MPa, a Young's modulus of 524.6 MPa, and an elongation at break of 11.27%.

Representative tensile stress–strain curves are shown in Figure 4.

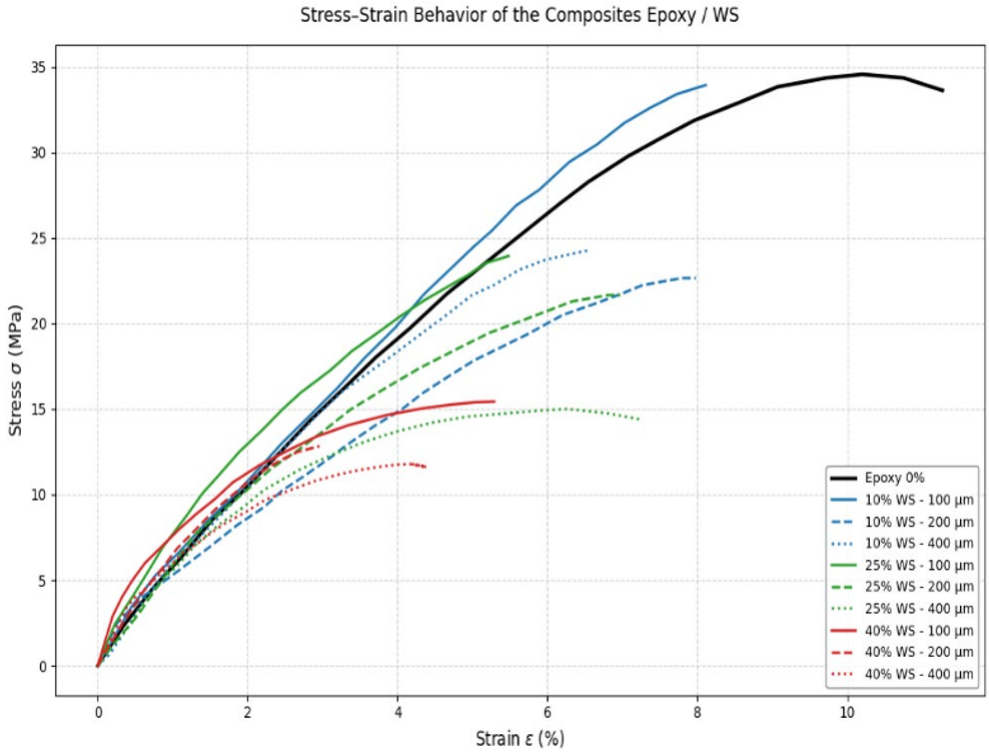


Figure 4. Tensile stress-strain curves for pure epoxy (E0) and nine reinforced formulations

Table 4. Tensile mechanical properties of epoxy/walnut shell powder composites

Code	σ_{exp} (MPa)	E_{exp} (MPa)	ε (%)
E0	34.56 ± 4.47	524.6 ± 21.6	11.27
E10-100	33.93 ± 2.76	714.2 ± 30.6	8.11
E10-200	22.65 ± 1.31	704.8 ± 12.2	7.98
E10-400	24.26 ± 1.98	604.6 ± 13.2	6.53
E25-100	23.94 ± 2.73	647.7 ± 17.6	2.74
E25-200	21.66 ± 2.55	559.3 ± 9.9	3.49
E25-400	15.00 ± 1.36	487.8 ± 12.6	3.62
E40-100	15.43 ± 1.87	930.3 ± 18.1	5.29
E40-200	12.83 ± 1.36	696.4 ± 8.4	2.96
E40-400	11.78 ± 0.28	700.4 ± 6.6	4.39

For all particle sizes, an increase in the mass fraction of the filler consistently reduces tensile strength, while 100 µm particles consistently exhibit the highest values for a given filler content. In contrast, Young's modulus increases with the incorporation of filler, reaching its maximum for the finest particles at the highest filler content. Elongation at break decreases with the addition of reinforcement, with the lowest values recorded at 25% and 40% by weight. All detailed numerical data are summarized in Table 4, while representative stress–strain curves are shown in Figure 4. The variation of Young's modulus as a function of filler content and particle size is illustrated in more detail in Figure 5.

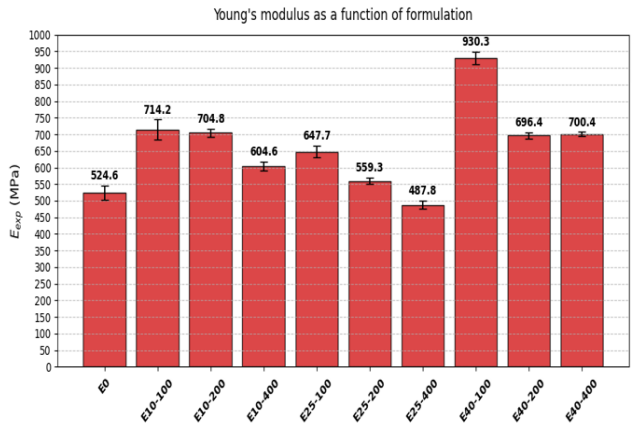


Figure 5. Tensile Young's modulus of epoxy/walnut shell powder composites

3.2 Compressive mechanical properties

The results of the compression tests are presented in Table 5. Neat epoxy shows an average maximum compressive stress of 55.34 ± 1.45 MPa.

Table 5. Average maximum compressive stress of epoxy/walnut shell powder composites

Code	σ_{comp} (MPa)	Variation vs E0 (%)
E0	55.34 ± 1.45	—
E10-100	57.94 ± 0.69	+4.70
E10-200	47.93 ± 2.07	−13.38
E10-400	33.32 ± 1.30	−39.79
E25-100	62.89 ± 1.08	+13.65
E25-200	50.69 ± 2.58	−8.41
E25-400	51.30 ± 1.17	−7.30
E40-100	60.55 ± 0.36	+9.42
E40-200	56.47 ± 1.04	+2.05
E40-400	35.01 ± 0.49	−36.73

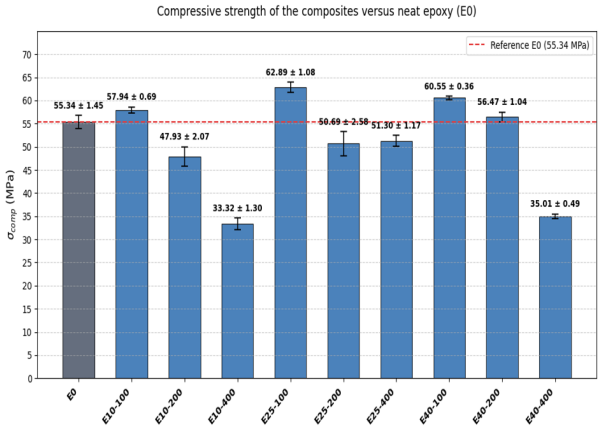


Figure 6. Compressive strength σ_{comp} of epoxy/walnut shell composites compared to neat epoxy (E0)

The compressive strength of each formulation is compared to neat epoxy in Figure 6.

The compressive strength is highly dependent on both particle size and filler content, as detailed in Table 5 and illustrated in Figure 6. The 100 µm particles systematically enhance the compressive strength relative to neat epoxy, with the best performance observed at 25 wt.% loading. In contrast, the 200 µm particles exhibit a progressive increase in strength with increasing filler content, approaching that of the neat matrix at 40 wt.%. The 400 µm particles lead to a substantial decrease at both low and high loadings, although a clear recovery is observed at the intermediate content. Overall, the 100 µm particles consistently deliver the best compressive performance across all filler loadings.

3.3 Statistical analysis of compressive strength

Table 6. Two-way analysis of variance (ANOVA) of the maximum compressive stress

Source of Variation	ddl	F	p-Value
Filler content (T)	2	201.72	$2.76 \times 10^{-20} < 0.001$
Particle size (G)	2	1144.73	$2.61 \times 10^{-33} < 0.001$
Interaction T × G	4	115.19	$5.38 \times 10^{-20} < 0.001$
Residuals	36		

The two-way ANOVA reveals highly significant effects of filler content, particle size, and their interaction (Table 6), justifying a post-hoc multiple comparison analysis. Tukey's test ($\alpha = 0.05$) identifies three statistically distinct performance groups (Table 7, Figure 7). The high-performance group consists exclusively of 100 µm formulations, with the highest strength at 25 wt.%. An intermediate group includes 200 µm formulations across all loadings, together with the 400 µm formulation at 25 wt.%. The lower group comprises 400 µm particles at both low and high contents, confirming their detrimental effect at extreme loadings. Notably, the 400 µm formulation at 25 wt.% stands out as a statistically significant exception, recovering to the intermediate level.

Table 7 presents the homogeneous groups resulting from Tukey's test. The letters assigned to each formulation allow direct interpretation of significant differences: two formulations sharing no common letter exhibit significantly different compressive strengths ($p < 0.05$).

The Tukey homogeneous groups are visualized in Figure 7.

Table 7. Homogeneous groups from Tukey's post-hoc test (HSD, $\alpha = 0.05$) for maximum compressive stress

Code	Stress (MPa)	Homogeneous Groups
E25-100	62.89 ± 1.08	a
E40-100	60.55 ± 0.36	a. b
E10-100	57.94 ± 0.69	b
E40-200	56.47 ± 1.04	b. c
E25-400	51.30 ± 1.17	c. d
E25-200	50.69 ± 2.58	d
E10-200	47.93 ± 2.07	d. e
E40-400	35.01 ± 0.49	f
E10-400	33.32 ± 1.30	f

Note: Honestly significant difference (HSD).

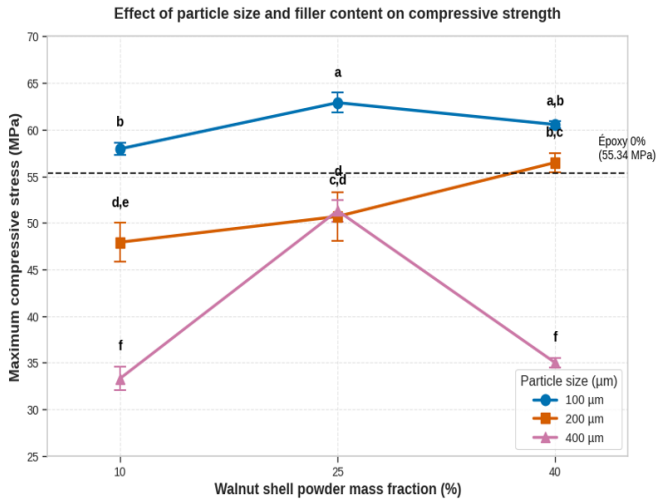


Figure 7. The maximal compressive stress of epoxy/walnut shell composites is influenced by mass fraction and particle size

Note: Tukey's HSD ($\alpha = 0.05$) distinguishes homogeneous groups (a–f), honestly significant difference (HSD).

3.4 Macroscopic observations of failure modes after compression

Two distinct damage modes are observed depending on the formulation. For the majority of formulations (100 µm and 200 µm), the specimens remain intact after testing despite significant deformation, with slight lateral buckling and a network of superficial oblique cracks relative to the loading axis. The specimens retain their structural continuity. For the E40-400 formulation, a different behavior is observed: a clear macroscopic fracture, with an oblique crack crossing the cylindrical section along a plane inclined at approximately 45° to the compression axis, causing partial separation of the two parts of the specimen. The fracture surface appears irregular. The two distinct failure modes are shown in Figure 8.

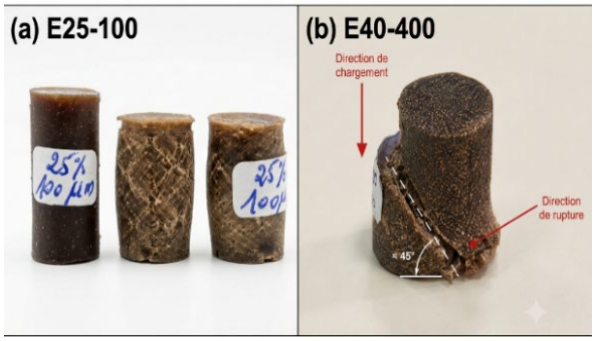


Figure 8. Compression failure modes: (a) E25-100 - ductile behavior with lateral buckling and superficial cracks without a clear fracture, and (b) E40-400 - brittle fracture along a shear plane inclined at approximately 45°

3.5 Comparison between experimental results and theoretical models

The elastic modulus values predicted by the Halpin–Tsai model [22, 23], as well as the tensile strengths estimated by the Pukánszky model [24], were compared with the experimental results. The relative deviation was calculated using Eq. (6).

$$Relative\ deviation(\%) = \frac{X_{exp} - X_{th}}{X_{th}} \times 100 \qquad (6)$$

Table 8. Comparison of experimental and predicted Young's moduli (Halpin–Tsai model)

Code	E_{th} (MPa)	E_{exp} (MPa)	Deviation (%)
E10-100	723.6	714.2 ± 30.6	−1.30
E10-200	723.6	704.8 ± 12.2	−2.60
E10-400	723.6	604.6 ± 13.2	−16.45
E25-100	1074.3	647.7 ± 17.6	−39.71
E25-200	1074.3	559.3 ± 9.9	−47.94
E25-400	1074.3	487.8 ± 12.6	−54.59
E40-100	1511.1	930.3 ± 18.1	−38.44
E40-200	1511.1	696.4 ± 8.4	−53.91
E40-400	1511.1	700.4 ± 6.6	−53.65

Table 9. Comparison of experimental and predicted tensile strengths (Pukánszky model)

Codes	σ_{exp} (MPa)	σ_{th} (MPa)	Deviation (%)
E10-100	33.93 ± 2.76	27.52	+23.29
E10-200	22.65 ± 1.31	25.66	−11.73
E10-400	24.26 ± 1.98	24.18	+0.33
E25-100	23.94 ± 2.73	21.74	+10.12
E25-200	21.66 ± 2.55	18.49	+17.14
E25-400	15.00 ± 1.36	16.12	−6.95
E40-100	15.43 ± 1.87	17.50	−11.83
E40-200	12.83 ± 1.36	13.76	−6.76
E40-400	11.78 ± 0.28	11.23	+4.90

Table 8 presents the comparison of the experimental Young's moduli with the Halpin–Tsai model predictions. Since this model depends only on the volume fraction V_f and not on particle size, the theoretical value Eth is identical for all three particle sizes at a given mass fraction.

The increasing deviation with V_f reflects the degradation of microstructural quality at high filler contents.

Table 9 presents the comparison of experimental tensile strengths with the predictions of the Pukánszky model. The values of the interaction parameter B used are 1.689 for 100 µm, 1.222 for 200 µm, and 0.827 for 400 µm.

The correlation between experimental and predicted tensile strengths is shown in Figure 9.

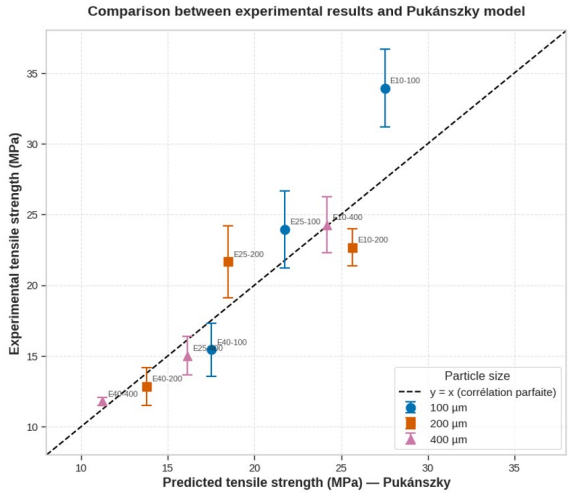


Figure 9. Experimental vs. Pukánszky-predicted tensile strength for 100, 200, and 400 µm particles
Note: Dashed line: perfect correlation; error bars: standard deviation (SD) (n = 5).

4. DISCUSSION

4.1 Stiffness strength trade-off and the role of the interface

Walnut shell powder creates a trade-off between stiffness and tensile strength. Fine 100 µm particles increase modulus by up to 77% at 40 wt.%, but tensile strength declines from 10 wt.% for all sizes, indicating insufficient interfacial adhesion without surface treatment. This contrasts with improvements after alkaline treatment [9] and with the optimum at 10 wt.% for date palm nut powder [15], suggesting surface chemistry and morphology influence adhesion. Our results align with untreated walnut shells [12], where strength decreases with filler content, especially for larger particles. Pukánszky parameter B decreases from 1.689 (100 µm) to 1.222 (200 µm) and 0.827 (400 µm). B integrates interface quality, dispersion, and porosity [24] and correlates with IFSS [25, 26]. Its decline reflects deteriorating load transfer due to weaker adhesion and stress concentrations. For 400 µm particles, lower specific surface area reduces contact with the matrix, while angular shape promotes local stress concentrations at corners. These effects initiate debonding at lower strains, explaining the early strength drop. In contrast, 100 µm particles, though untreated, offer larger specific surface area and more uniform distribution, delaying debonding and allowing better stress transfer up to higher filler contents.

4.2 Ductile-to-brittle transition in compression

Under compression, the response is governed by coupled particle size and filler content, confirmed by significant ANOVA interaction ($p < 0.001$). 100 µm formulations retain ductile behaviour with lateral buckling and superficial cracking but no sudden failure. This ductility allows the high-performance group (57.9–62.9 MPa) to exceed neat epoxy (55.34 MPa) due to relatively homogeneous dispersion and effective load transfer, delaying damage localization. In contrast, 400 µm particles at 10 and 40 wt.% trigger brittle

shear failure with oblique cracking at ~45° and a sharp strength drop (33.3–35.0 MPa). Coarse particles act as stress concentrators, promoting early interfacial crack initiation and coalescence into a macroscopic shear plane. Macroscopic failure modes in Section 3.4 support this: ductile 100 µm formulations distribute damage without a continuous crack path, while brittle E40-400 forms a clean oblique fracture plane, suggesting coarse particles localise damage and allow rapid crack propagation. Although no SEM images confirm microscale mechanisms, macroscopic evidence is consistent with proposed roles of particle size and interfacial quality. E25-400 (51.30 MPa) is a notable exception ($p < 0.05$), falling in the intermediate group. At $V_f = 0.346$, favourable particle arrangement and possibly reduced local porosity may offset interfacial defects. However, absence of direct microstructural evidence limits confirmation—a limitation for future work.

4.3 Validation of micromechanical models

Halpin–Tsai model [22, 23] increasingly overestimates Young's modulus with filler content, with deviations up to −55% at 40 wt.%. This cannot be attributed solely to agglomeration or porosity. The model assumes perfect interfacial adhesion and spherical particles ($\xi = 2$), whereas walnut shell powder is angular and irregular, and the untreated interface provides limited stress transfer. These factors explain much of the deviation. The model was chosen for simplicity and low data requirements, advantageous without detailed microstructural characterization. However, the magnitude of deviation at high loadings suggests it is inappropriate beyond a certain volume fraction. Alternative models, such as Lewis–Nielsen with maximum packing fraction and interface-based homogenization models [27], could be explored in future work.

Pukánszky model [24] correlates much better with tensile strength. Deviations range from +23.3% (underestimation) to −11.8% (overestimation), with near-perfect prediction for E10-400 (+0.3%). It performs well for coarse particles at low content, close to its assumptions (quasi-spherical particles, weak inter-particle interactions). Underestimation for fine particles at 10% suggests more effective load transfer than predicted by B, possibly due to high specific surface area, while overestimation at 40% reflects imperfections (agglomerates, porosities) reducing actual strength.

4.4 Limitations and outlook

Several limitations should be acknowledged. First, absence of filler surface treatment limits tensile performance; alkalization or silanization could enhance interfacial adhesion and raise B. Second, microstructural characterization was restricted to macroscopic observations. No SEM imaging, porosity mapping, or quantitative particle size distribution after processing was possible due to equipment limitations. These analyses are essential to confirm proposed mechanisms and will be addressed in future work. Third, particle dispersion was assessed only visually; no microscopic or experimental quantification was possible. Fourth, rheological control of dispersion and optimization of mixing protocol require further investigation to push back the agglomeration threshold at high volume fractions. Future work should incorporate porosity and a dispersion parameter into Halpin–Tsai and Pukánszky models to improve accuracy for these bio-based composites. A systematic study of surface treatments across particle sizes will be a logical next step toward high-performance materials balancing stiffness, strength, and durability.

5. CONCLUSIONS

This study evaluated the combined influence of particle size (100, 200, 400 µm) and mass fraction (10, 25, 40%) of walnut shell powder on mechanical properties of epoxy composites. Interaction determines elastic properties, ultimate strength, and damage mode. Fine 100 µm particles enabled maximum Young's modulus of 930 MPa (+77%) while maintaining ductile compressive behaviour even at 40% loading (60.55 MPa). In contrast, 400 µm particles led to an early drop in tensile strength and sharp transition to brittle shear failure in compression at 40% (35.01 MPa, −37%). Two-way ANOVA ($p < 0.001$) followed by Tukey's test identified three distinct performance groups, confirming significant effects of particle size, filler content, and interaction. Experimental data revealed increasing deviations from Halpin–Tsai and Pukánszky models at higher volume fractions. Main limitations are the absence of surface treatment and detailed microstructural characterization. Future work should focus on chemical interface modification (alkalization, silanization) and integration of microstructural defects into enriched models.

ACKNOWLEDGMENTS

The authors would like to express their gratitude to their thesis director and co-supervisors for their advice, encouragement, and insightful criticism during this study. Their knowledge and counsel were very helpful in advancing and finishing this project.

REFERENCES

[1] Faruk, O., Bledzki, A.K., Fink, H.P., Sain, M. (2012). Biocomposites reinforced with natural fibers: 2000–2010. Progress in Polymer Science, 37(11): 1552-1596. https://doi.org/10.1016/j.progpolymsci.2012.04.003

[2] Mahmud, M.Z.A., Rabbi, S.F., Islam, M.D., Hossain, N. (2025). Synthesis and applications of natural fiber-reinforced epoxy composites: A comprehensive review. SPE Polymers, 6(1): e10161. https://doi.org/10.1002/pls2.10161

[3] Elfaleh, I., Abbassi, F., Habibi, M., et al. (2023). A comprehensive review of natural fibers and their composites: An eco-friendly alternative to conventional materials. Results in Engineering, 19: 101271. https://doi.org/10.1016/j.rineng.2023.101271

[4] Pickering, K.L., Efendy, M.A., Le, T.M. (2016). A review of recent developments in natural fibre composites and their mechanical performance. Composites Part A: Applied Science and Manufacturing, 83: 98-112. https://doi.org/10.1016/j.compositesa.2015.08.038

[5] Kabir, M.M., Wang, H., Lau, K.T., Cardona, F. (2012). Chemical treatments on plant-based natural fibre reinforced polymer composites: An overview. Composites Part B: Engineering, 43(7): 2883-2892. https://doi.org/10.1016/j.compositesb.2012.04.053

[6] Manterola-Barroso, C., Padilla Contreras, D., Ondrasek, G., Horvatinec, J., Gavilán CuiCui, G., Meriño-Gergichevich, C. (2024). Hazelnut and walnut nutshell features as emerging added-value byproducts of the nut industry: A review. Plants, 13(7): 1034. https://doi.org/10.3390/plants13071034
[7] Salih, H. (2020). Physicochemical properties of walnuts (Juglans regia L.) shells and kernels growing in different locations in Kurdistan region-Iraq. Journal of Zankoy Sulaimani-Part A, 22: 109-118. https://doi.org/10.17656/jzs.10812
[8] Antreich, S.J., Xiao, N., Huss, J.C., Horbelt, N., Eder, M., Weinkamer, R., Gierlinger, N. (2019). The puzzle of the walnut shell: A novel cell type with interlocked packing. Advanced Science, 6(16): 1900644. https://doi.org/10.1002/advs.201900644
[9] Shejkar, S.K., Agrawal, B., Agrawal, A., Gupta, G. (2022). Physical, mechanical, and sliding wear behavior of epoxy composites filled with surface modified walnut shell particulate. Polymer Composites, 43(10): 7526-7537. https://doi.org/10.1002/pc.26847
[10] Karagöz, İ., Mutlu, D., Çavuşoğlu, A., Çelebi, M., Ceylan, Ö. (2025). A comprehensive study on the effect of small rates of walnut shell and talc fillers on the thermal, mechanical, and morphological properties of epoxy hybrid composites. Biomass Conversion and Biorefinery, 15(6): 8439-8450. https://doi.org/10.1007/s13399-024-05660-9
[11] Shejkar, S.K., Agrawal, B., Agrawal, A. (2021). Influence of the size of walnut shell particulates on mechanical properties of epoxy-based composites. Journal of Engineering Research. https://doi.org/10.36909/jer.ICIPPSD.15541
[12] Salasinska, K., Barczewski, M., Górny, R., Kloziński, A. (2018). Evaluation of highly filled epoxy composites modified with walnut shell waste filler. Polymer Bulletin, 75(6): 2511-2528. https://doi.org/10.1007/s00289-017-2163-3
[13] Pradhan, P., Satapathy, A. (2022). Physico-mechanical characterization and thermal property evaluation of polyester composites filled with walnut shell powder. Polymers and Polymer Composites, 30: 09673911221077808. https://doi.org/10.1177/09673911221077808
[14] Koyunucu, M., Ulay, G. (2023). Thermal and flammability behavior of walnut shell reinforced epoxy composites. Polímeros, 33(2): e20230018. https://doi.org/10.1590/0104-1428.20230018
[15] Chaoufi, A., Benzegaou, A., Badraoui, A. (2025). Mechanical characterization of date palm nut powder reinforced composite material from Bechar Algeria Region. Revue des Composites et des Materiaux Avances, 35(2): 375-380. https://doi.org/10.18280/rcma.350219
[16] EPODEX. (2026). ECO system – Epoxy resin for castings up to 1 cm. https://www.epodex.com/en/product/eco-system/.
[17] European Pharmacopoeia Commission. (2023). European pharmacopoeia (11th ed., chap. 2.2.32, loss on drying). Strasbourg: EDQM.
[18] Pączkowski, P. (2023). Properties of eco-friendly composites based on post-consumer recycled resin filled with walnut shell powder. Polymers, 15(22): 4389. https://doi.org/10.3390/polym15224389
[19] Beskopylny, A.N., Stel'makh, S.A., Shcherban', E.M., et al. (2023). Effect of walnut-shell additive on the structure and characteristics of concrete. Materials, 16(4): 1752. https://doi.org/10.3390/ma16041752
[20] ASTM International. (2022). ASTM D638-22: Standard test method for tensile properties of plastics. ASTM International. https://doi.org/10.1520/D0638-22
[21] ASTM International. (2026). ASTM D695-26: Standard test method for compressive properties of rigid plastics. ASTM International. https://doi.org/10.1520/D0695-26
[22] Affdl, J.H., Kardos, J.L. (1976). The Halpin-Tsai equations: A review. Polymer Engineering & Science, 16(5): 344-352. https://doi.org/10.1002/pen.760160512
[23] Shokrieh, M.M., Moshrefzadeh-Sani, H. (2016). On the constant parameters of Halpin-Tsai equation. Polymer, 106: 14-20. https://doi.org/10.1016/j.polymer.2016.10.049
[24] Pukanszky, B. (1990). Influence of interface interaction on the ultimate tensile properties of polymer composites. Composites, 21(3): 255-262. https://doi.org/10.1016/0010-4361(90)90240-W
[25] Zare, Y., Rhee, K.Y. (2020). Effects of critical interfacial shear strength between polymer and nanoclay on the Pukanszky's "B" interphase factor and tensile strength of polymer nanocomposites. Mechanics of Materials, 149: 103562. https://doi.org/10.1016/j.mechmat.2020.103562
[26] Lazzeri, A., Phuong, V.T. (2014). Dependence of the Pukánszky's interaction parameter B on the interface shear strength (IFSS) of nanofiller-and short fiber-reinforced polymer composites. Composites Science and Technology, 93: 106-113. https://doi.org/10.1016/j.compscitech.2014.01.002
[27] Fedotov, A. (2018). Interface model of homogenization for analysing the influence of inclusion size on the elastic properties of composites. Composites Part B: Engineering, 152: 241-247. https://doi.org/10.1016/j.compositesb.2018.07.007

NOMENCLATURE

B	Pukánszky interaction parameter, dimensionless
E_c	Young's modulus of the composite, Pa
E_{exp}	Experimental Young's modulus, Pa
E_f	Young's modulus of the reinforcement (walnut shell), Pa
E_m	Young's modulus of the epoxy matrix, Pa
E_{th}	Theoretical Young's modulus (Halpin–Tsai model), Pa
n	Number of specimens per formulation, dimensionless
V_f	Volume fraction of the reinforcement, dimensionless
V_m	Volume fraction of the matrix, dimensionless
ε	Elongation at break, %
η	Auxiliary parameter of the Halpin–Tsai model, dimensionless
ξ	Shape parameter of the Halpin–Tsai model, dimensionless
ρ_f	Density of the reinforcement (walnut shell), kg·m^{-3}
ρ_m	Density of the epoxy matrix, kg·m^{-3}

σ_{comp} Maximum compressive stress, Pa
σ_c Tensile strength of the composite, Pa
σ_{exp} Experimental tensile strength, Pa
σ_m Tensile strength of the epoxy matrix, Pa
σ_{th} Theoretical tensile strength (Pukánszky model), Pa
ω_f Mass fraction of the reinforcement, dimensionless
ω_m Mass fraction of the matrix, dimensionless